JOURNAL OF MATERIALS SCIENCE 25 (1990) 3385–3395

Structure–property relations in an injection-moulded, rubber-toughened, semicrystalline polyoxymethylene

T. J. PECORINI, R. W. HERTZBERG, J. A. MANSON
Department of Materials Science and Engineering, Lehigh University, Bethlehem, Pennsylvania 18017, USA

A relationship has been identified between the injection-moulded structure of a rubber-toughened polyoxymethylene (POM), and its mechanical properties. The material used was a commercially available POM (Dupont ST100) which contained 20% to 30% polyurethane rubber within a 50% to 60% crystalline matrix. These percentages were invarient through the thickness. A strong sensitivity towards the development of a core–skin morphology was discovered; microscopy and microhardness techniques revealed the skin depth to be 1200 μm. The skin layer was found to consist of individual sheets, 2 to 4 μm thick, that were stacked parallel to the plaque face. By contrast, the core contained spherulites, of 100 to 300 μm diameter, that surrounded oriented discrete 2 to 4 μm thick rubber rods. Morphological differences between the core and skin were reflected in their respective mechanical properties. Tensile response in the skin was ductile, with elongations reaching 300%, while the core exhibited more brittle behaviour (only 25% elongation). In both regions the yield strength was 45 MPa, a value expectedly reduced from the homopolymer (69 MPa) due to the presence of the rubber phase. Fatigue crack propagation response in the skin of the blend was found to be superior to that of the neat resin; however, the core behaviour was a function of orientation. A combination of inferior FCP response and the noticeable presence of a preferred plane of fracture, highlighted the significant weakness of the core material when loaded in a direction transverse to the injection moulding direction.

1. Introduction

A basic understanding of a material's response to both static and cyclic loading is essential in predicting its behaviour for a wide variety of engineered applications. Tensile and fatigue tests provide both analytical data as well as an indication of whether the material will behave in a ductile or brittle manner. The former is useful in part design and manufacture, while the latter is important for material design and fracture control.

The alternative conditions of either ductile (tough) or brittle behaviour are controlled by the material's composition and morphology [1–3]. In polymeric systems, factors which restrict widespread yielding, such as high entanglement densities (or cross-links), large spherulite size, or coarse inclusion distributions, prevent diffuse shear yielding and embrittle the polymer. In contrast, the addition of finely distributed second-phase rubber particles, high temperatures, low strain rates, and a biaxial (rather than triaxial) stress state, dissipate the applied strain energy, and initiate ductile behaviour. Ductile systems are less subject to the catastrophic failure, but they also possess lower strength levels.

While compositional control may be easily obtained, a material's morphology is usually determined by the processing technique utilized. In polymer systems, one of the most common fabrication methods is injection moulding. This technique, while very simple in operation, subjects the polymer to a complex environment of stresses and thermal gradients [4–6]. Near the mould walls, the material, highly stressed along the direction of injection, is flash-frozen by the rapid cooling rates. This forms the skin zone. In the centre or core of the moulding, slower cooling rates permit Brownian relaxation to occur, thereby resulting in a randomly oriented morphology.

The morphological differences between the core and skin are reflected in their respective mechanical properties; the slowly cooled, coarse structures within the core are often brittle, while the quenched, finer morphologies in the skin are often ductile. The overall mechanical behaviour of an injection moulding is, therefore, a function of the relative properties and volume fraction of these two regions [7–14]. This dependence of mechanical properties on the core/skin ratio implies that information gathered from thin injection-moulded tensile bars may improperly describe the properties of thick injection-moulded or compression-moulded parts, thereby leading to non-conservative design assessments. Understanding the relationship between the core–skin morphology and

0022–2461/90 $03.00 + .12

mechanical properties of a particular polymer system is, therefore, essential before laboratory data can be incorporated into part design.

This core–skin morphology has been detected in a variety of polymer systems including amorphous [4, 15, 16], semicrystalline [5, 7–11, 17, 18], short fibre-reinforced [12, 19, 20] and rubber-toughened resins [13, 21–23]. In systems possessing discrete structures, the most economical microstructural detection methods are often simple metallographic analyses. These techniques involve either light-optical or electron microscope examination of polished samples treated with either acid etches, solvytic extraction, or by staining sensitive phases with osmium tetroxide. Another simple method of locating different microstructures within a sample is through microhardness testing [17, 18, 24, 25]. Such a method detects not only variations in the deformability of different microstructures, but may also reveal anisotropy in the residual microhardness indentations for materials that possess non-uniform morphologies.

The most complex core–skin morphologies arise in systems which possess both crystalline and rubber phases. Of these materials, rubber-toughened polyoxymethylene (HI-POM), reportedly one of the toughest of all polymer systems [26–29], is among the newest and least understood. This makes HI-POM an excellent candidate for study. Although very little information has been published on this material, it can be inferred from the patent literature [27–29] that this polymer alloy contains 25% to 32% polyurethane rubber, arranged either as spheres, rods, or in a semi-interpenetrating network. The matrix material is believed to be the same as that used in Delrin 100 (molecular weight 70 000). Note that the neat Delrin is known to possess a very definite core–skin morphology when injection moulded, with a skin depth of 300 μm [8, 30]. In an attempt to understand better both the structure of the HI-POM material and its extraordinary properties, the structure–property relations for this HI-POM material have been characterized in a series of compositional, microstructural and mechanical analyses.

2. Experimental procedure

2.1. Materials

The materials tested were commercial grades of semicrystalline polyoxymethylene. The neat POM (DuPont Delrin 100) and the rubber-toughened version (ST100) were supplied in end-gated, injection-moulded, rectangular plaques, 3.2 and 6.4 mm thick. The nominal planar dimensions of the plaques were 8 cm × 20 cm and 10 cm × 40 cm for the neat and HI-POM materials, respectively. The exact thermal histories of the plaques were unknown but were reportedly produced under commercial fabrication conditions [31] and did not vary between samples tested in this study.

2.2. Dynamic mechanical spectra, differential scanning calorimetry and density

Dynamic mechanical spectra (DMS) were obtained from specimens which were saw-cut and hand-sanded to dimensions of 1 cm × 0.5 cm × 7 cm. Testing was performed in air at 110 Hz using an Autovibron unit, model DDV-IIIC. Data were obtained over a temperature range of −120 to 200° C at a heating rate of 1° C min^{-1}. Glass transition and melting temperatures(T_g and T_m, respectively) were taken as the values of temperature corresponding to the maximum in the major peaks of the tan δ curves. Tan δ is defined as the ratio of loss to storage moduli (E''/E').

Differential scanning calorimetry (DSC) was used to confirm the transition temperatures identified by DMS and to determine the per cent crystallinity of the matrix. DSC was performed with a Mettler TA3000 balance calibrated with indium, on samples hand cut from multiple locations through the thickness of the plaques. Analysis was performed on 5 to 10 g samples, in air, over a range of −100 to 240° C, at a scanning rate of 10° C min^{-1}. The per cent crystallinity was determined by comparing the heat of fusion (H_f) per gram calculated from the DSC plot with a value of H_f per gram for 100% crystalline material. The value of H_f for 100% crystalline POM was 250 J g^{-1}, as noted in the Mettler User Guide [32].

Density measurements were performed by Archimedes principle as given in ASTM D792-66 [33] and measurements were evaluated to four significant figures. Samples for testing were hand cut from various locations through the thickness of the plaques.

2.3. Microscopy

Polymer morphology was examined on polished and treated samples using either a Zeiss Axiomat light optical microscope or an ETEC autoscan scanning electron microscope (SEM). For the latter, a 10 kV accelerating voltage was used in order to minimize beam damage. Prior to SEM investigation, specimens were sputter-coated with gold–palladium to a thickness of 25 μm.

Polishing followed standard metallographic procedures, and a final polish with 0.5 μm alumina was found to be sufficient. Etching was performed by placing a drop of 70% nitric acid on a sample for 60 sec. (Alternatively, a dilute acid could be applied for a greater duration). Osmium-stained samples were prepared by immersion in a 1% solute of osmium tetroxide in dimethyl formamide (DMF) for 8 h. All treatments were performed at room temperature. The rubber morphology was also identified in specimens which had been subjected to standard tensile and fatigue tests. These fracture surfaces were examined in the untreated condition.

2.4. Microhardness testing

Samples for microhardness testing were cut from the injection-moulded plaques, mounted in epoxy to prevent edge rounding, and polished to improve visual resolution of the indentations. Measurements were taken at 0.5 mm intervals across the thickness with the indentors oriented orthogonal to the plaque faces. A 4 sec loading time was maintained throughout the testing programme, and the indentation lengths were measured within 30 sec after the removal of load.

Testing was performed on a Leco model M-400FT machine.

Impressions were made with both Vickers and Knoop indentors, with the following relations [34] used to evaluate the local compressive stresses involved

$$\text{Vickers Hardness (HV)} = \frac{P}{0.54\ D_1 D_2} \quad (1)$$

$$\text{Knoop Hardness (HK)} = \frac{P}{0.070\ L^2} \quad (2)$$

where P is the load in kg, and D_1, D_2, and L are the diagonal lengths in mm. 150 and 200 g loads were used for Knoop and Vickers indentations, respectively.

2.5. Mechanical properties

In order to characterize properly the mechanical behaviour of the core and skin morphologies, tensile and fatigue tests were performed on samples machined from both plaque thicknesses, and at orientations both parallel and perpendicular to the injection-moulding direction. Because the skin depth was found to be 1200 to 1500 μm, and did not vary between plaque thicknesses, the 3.2 mm thick as-moulded samples were considered to represent an all skin structure. Alternatively, 6.4 mm samples with the outer 1.6 mm removed from both sides represented core samples. Note that the "skin" and "core" samples were both nominally 3.2 mm thick; this would eliminate the question of whether a difference in thickness-related stress-state would affect the fatigue results. In addition, 6.4 mm as-moulded samples were tested to represent a material which contained equal amounts of core and skin morphologies (50/50 samples).

In order to compare the mechanical properties of the neat and toughened resins, data for unmodified POM are included in the test results. These data were taken from 6.4 mm thick samples which contained only 12% skin (as determined by microscopy) [30]. During both fatigue and tensile testing, these samples behaved in an isotropic manner.

Tensile properties were obtained on an Instron screw-driven tensile machine at a constant cross-head speed of 12.7 mm min^{-1}. Standard ASTM type V tensile bars were machined from the injection-moulded plaques and tested per ASTM D638-68 [35].

Fatigue crack propagation studies were conducted as per ASTM E399-86a [36] using an Instron servo-hydraulic closed-loop testing machine. Crack length measurements were noted either visually by travelling microscope, or were inferred from a compliance-based computer program. All waveforms were sinusoidal with an R-ratio (minimum load/maximum load) of 0.1, and all tests were conducted in laboratory air at ambient temperature.

Crack growth rates, da/dn, were correlated with ΔK, the stress intensity factor range using the Paris relation [2]

$$\frac{da}{dn} = A\Delta K^m \quad (3)$$

where A and m are material constants that depend also on test variables such as frequency, mean stress and environment. ΔK is defined [2] as

$$\Delta K = Y\Delta\sigma a^{1/2} \quad (4)$$

where Y is a geometrical factor, $\Delta\sigma$ is the range of applied stress, and a is the crack length. The majority of fatigue testing was performed at 5 Hz on wedge opening loaded (WOL) samples, for which the geometry factor [2] is

$$Y = \frac{(2 + a/W)}{(1 - a/W)^{3/2}}\left(\frac{W}{a}\right)^{1/2}\left[0.8072 + 8.858\left(\frac{a}{W}\right) - 30.23\left(\frac{a}{W}\right)^2 + 41.088\left(\frac{a}{W}\right)^3 - 24.15\left(\frac{a}{W}\right)^4 + 4.951\left(\frac{a}{W}\right)^5\right] \quad (5)$$

One test was performed at 10 Hz on a single-edge notched (SEN) sample in order to maintain in-plane crack growth. (Because the SEN stress field exists only in the direction of the applied load, no secondary driving force exists which can permit a crack growth out of plane). The geometry factor, Y, for the SEN configuration [2] is

$$Y = \left[1.99 - 0.41\left(\frac{a}{W}\right) + 18.7\left(\frac{a}{W}\right)^2 - 38.48\left(\frac{a}{W}\right)^3 + 53.85\left(\frac{a}{W}\right)^4\right] \quad (6)$$

3. Results and discussion

3.1. Compositional characterization

Fig. 1 shows the dynamic mechanical spectra for both the neat POM and HI-POM resins. Note that the tan δ curves for both materials contain peaks at -65 and 175° C, corresponding to the T_g and T_m, respectively, of the matrix POM. (This matrix T_g corresponds to the gamma relaxation, consistent with the literature [37]; no beta peak is present). The tan δ peak at -35° C, which is only present in the HI-POM material, must correspond to the T_g of the rubber phase. These transformation temperatures, confirmed with DSC data,

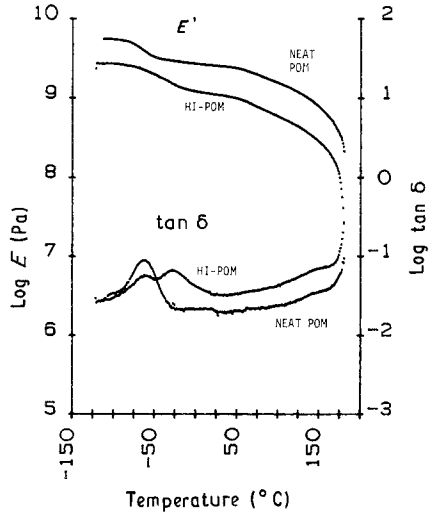

Figure 1 Dynamic mechanical spectra for both neat and rubber-toughened polyoxymethylene.

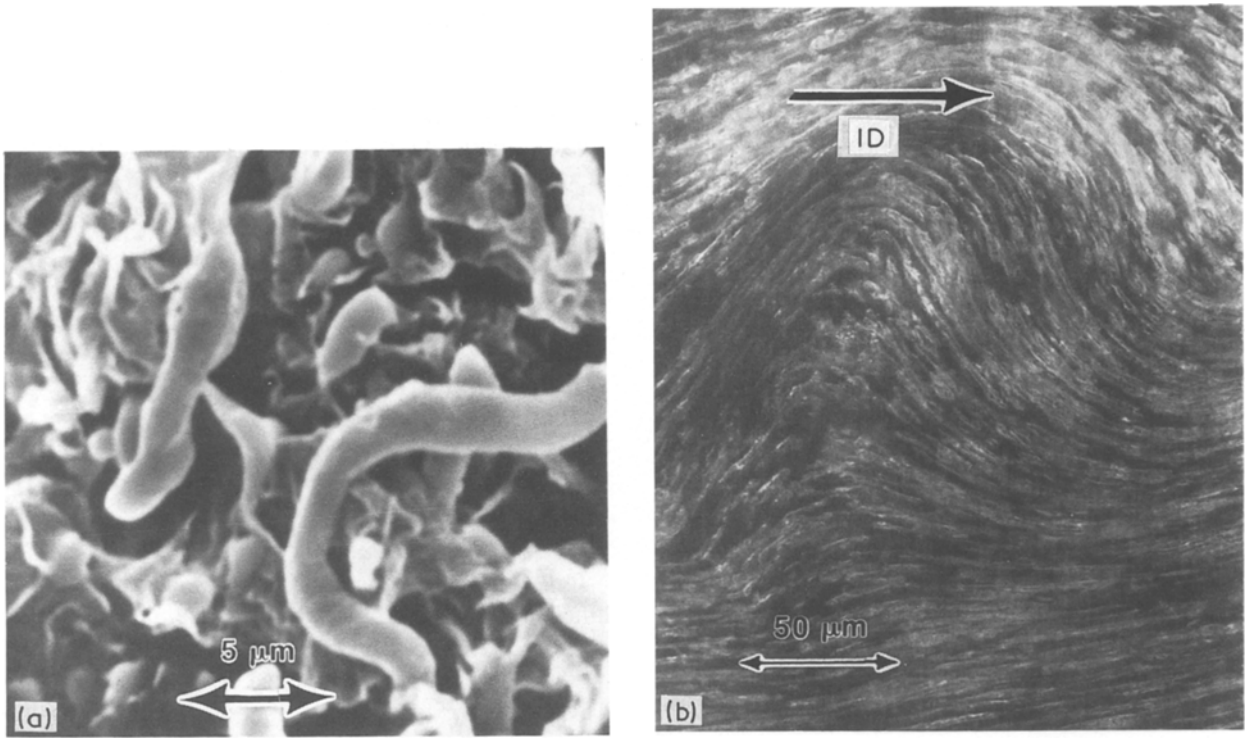

Figure 2 (a) Fatigue fracture surface showing large rod-like rubber particles in the centre of a 6.4 mm HI-POM sample. (b) Optical micrograph of a longitudinal section of HI-POM material. Sample has been polished and stained to reveal the orientation of the rubber phase along the direction of injection, following lines of turbulence.

support information from the original patents for the material [27–29] which suggests that the toughening agent is a polyurethane rubber with a T_g of $-35°C$.

Density and DSC measurements, combined with simple rule of mixtures calculations, revealed that both the HI-POM matrix polyomethylene and the neat POM resin are 50% to 60% crystalline. These measurements also confirm [27–29] that the HI-POM material contains 20% to 30% rubber. It is not possible to derive more exact values for the ratios of these two phases, because these calculations are dependent upon the values of density for the rubber and amorphous matrix, and the per cent crystallinity of polyoxymethylene, all of which may change slightly due to the mixing of the two polymers. Despite the inaccuracy in calculations, however, the measured values of both the percentage of rubber and the per cent crystallinity do not vary through the thickness. Thus, any changes in properties through the thickness cannot be caused by changes in composition, and must be purely morphological in origin.

3.2. Rubber morphology

Examination of both osmium-stained samples and fracture surfaces of the HI-POM material revealed the presence of many high-aspect-ratio stringers of rubber. It has been suggested that in this toughened material, the morphology of the rubber and matrix may be an interpenetrating network (IPN) [27–29]. However, DMS curves for the HI-POM do not show a merging of the two respective component T_g peaks, a characteristic feature of IPN structures. It is more probable that the thermodynamically stable morphology for the rubber in this blend is a simple rod-like arrangement. These rubber particles are found to be more coarsely distributed in the centre of the moulding, due to the decreasing cooling rate through the thickness; the micrographs in Figs 2 and 3 reveal that the diameter of the rubber domains increases from 0.3 μm near the edge of the moulding, to 3 μm at the centre. It is also apparent from Figs 2 and 3 that these rubber rods are aligned in the direction of flow, even to the point of following lines of turbulence.

3.3. Core–skin matrix morphology

The core–skin morphology of an etched 6.4 mm HI-POM sample is clearly shown in Fig. 4a. Closer examination of the core (Fig. 4b) reveals that the matrix is spherulitic in nature with the size of the spherulites averaging 200 μm. It is interesting to note that these spherulites are larger than those in the neat material (50 to 100 μm), a consequence of the rubber-induced reduction in the rate of crystallization as mentioned by Flexman [27–29]. Similar reductions in crystallization rates have been observed in other immiscible polymer blends, and is reportedly controlled by the thermodynamics of mixing between the two polymers [38]. Note, however, that the addition of rubber particles to other semicrystalline systems, such as Nylon, may cause the matrix spherulite size to be decreased [39].

In the skin of the HI-POM material, a sheet-like structure is observed (Fig. 4c, d). These 2 to 4 μm thick sheets appear to consist of very small crystalline domains bound together by a tight rubber network. The formation of this type of structure is presumably favoured by interaction between the slowly crystallizing matrix and the rapidly cooled, finely distributed rubber particles. Furthermore, due to the injection flow these sheets are stacked parallel to the plaque

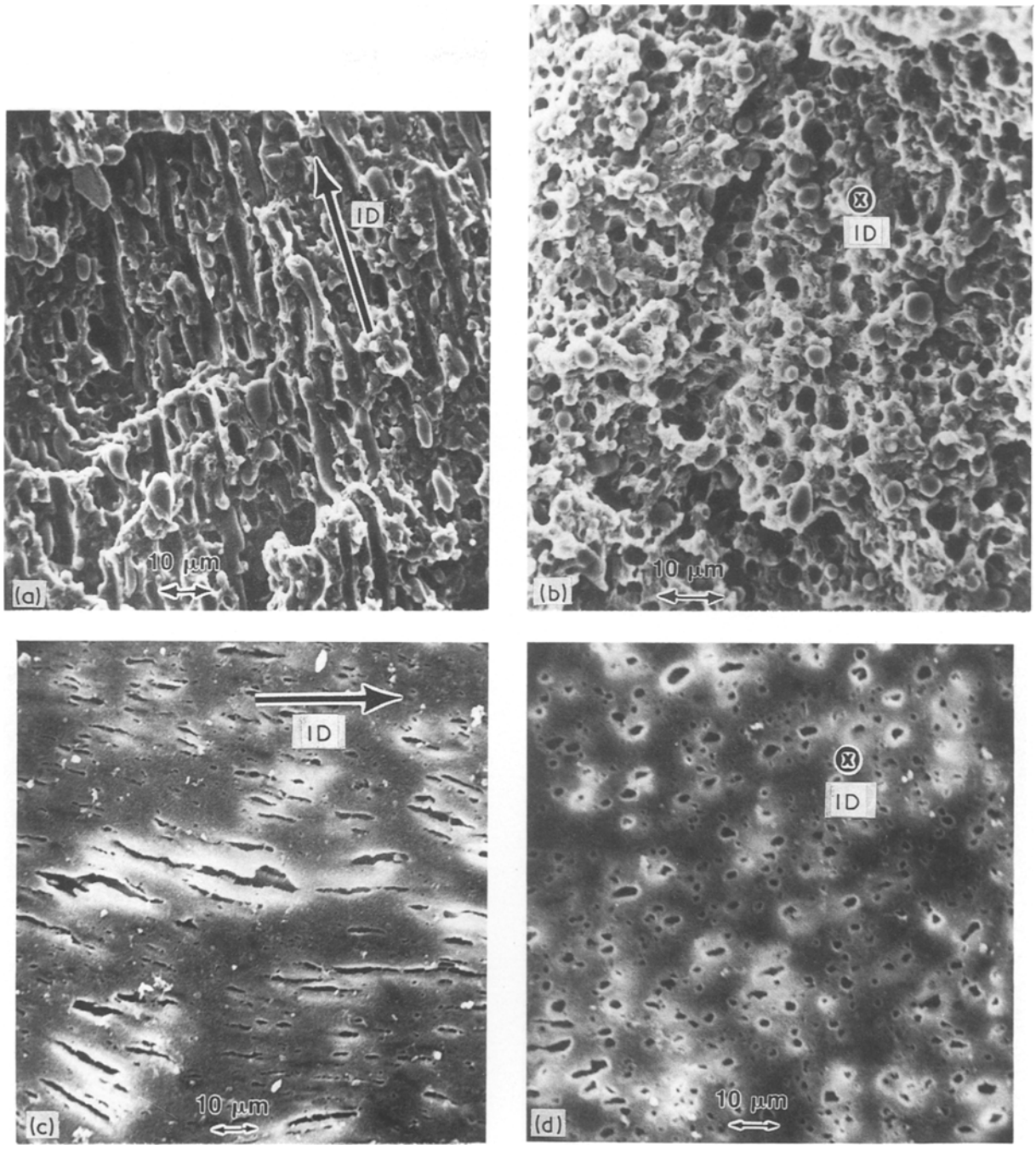

Figure 3 (a, b) Fracture surfaces in HI-POM core fast-fracture region. Note alignment of rubber rods (a) along the injection direction, and (b) end-on view of the rods. (c, d) Optical micrograph of polished and stained HI-POM samples showing (c) alignment of the rubber along the longitudinal direction, and (d) the cross-sectional holes in the transverse direction.

face, and are subject to delamination, as observed in both etched and fractured samples.

These weakly bonded sheets in the skin are easily pried apart by Vickers and Knoop microhardness indentors. Fig. 5a shows a Vickers trace across the thickness of a 6.4 mm HI-POM sample. The two sets of data corresponds to measurements taken from indentor diagonals oriented parallel to the plaque face, and normal to this direction. (Recall that the microhardness numbers are a function of the inverse square of the measured lengths). Close to the centre, both the parallel and perpendicular measurements are the same. In the skin region, however, the residual perpendicular indentation is observed to be longer than the parallel indentation due to additional deformations associated with sheet delamination.

Conversely, the knife-like Knoop indentor slides easily between the sheets, leaving a large indentation in the parallel direction (○); penetration across the structure is more difficult and results in a short perpendicular indentation (×). Note that for Knoop testing, two separate impressions must be made at each location, with each impression normal to the other. Note in Fig. 5b that the readings in the core were isotropic. As shown in Fig. 5c, superposition of the hardness data from Fig. 5b upon a micrograph of an etched 6.4 mm sample (recall Fig. 4a) provides excellent agreement between changes in the Knoop hardness values and the micromorphology of the blend.

Correlation between microhardness and microscopic analysis reveals that the skin for the HI-POM extended from the surface to a depth of 1200 to 1500 μm. This

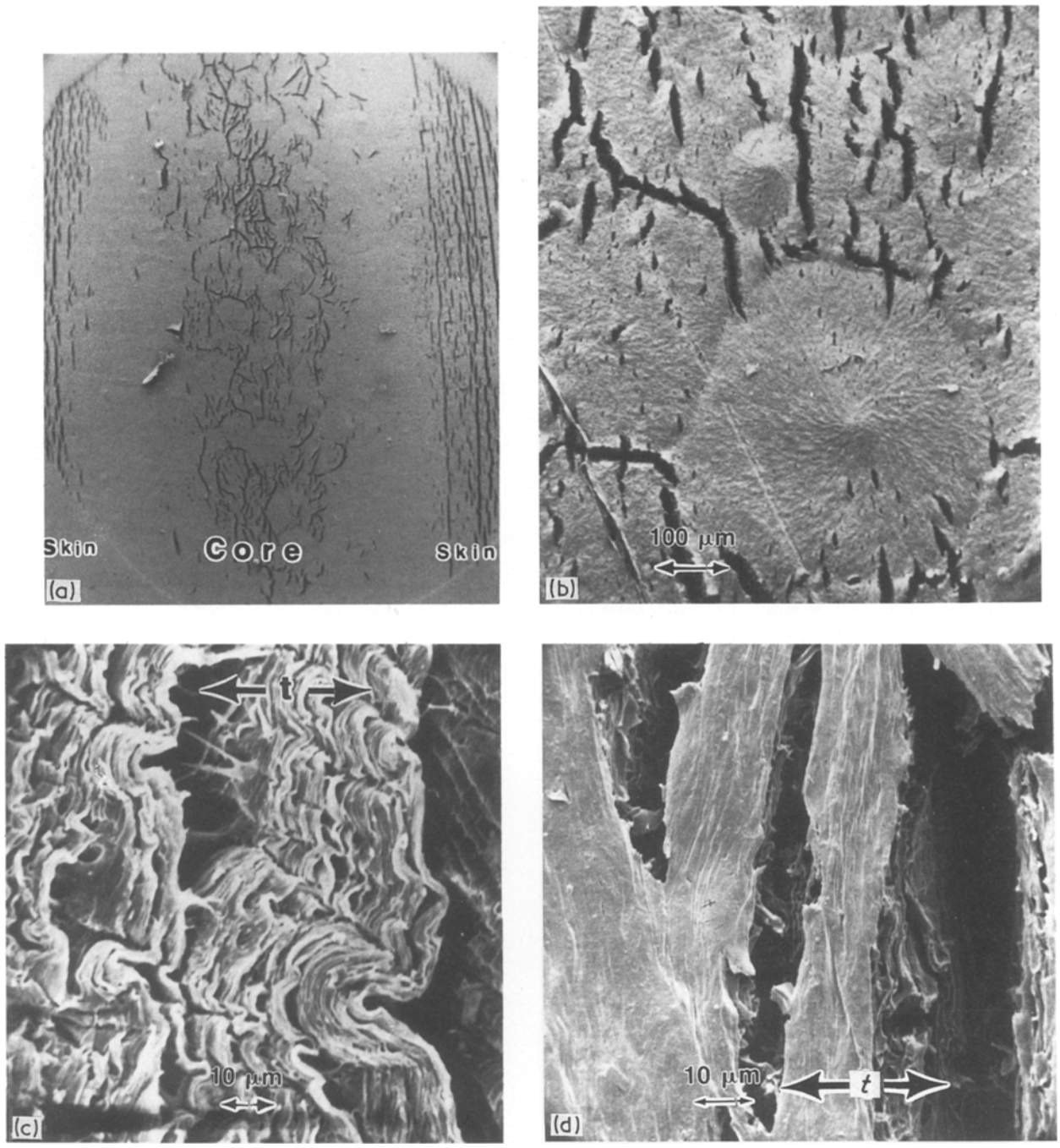

Figure 4 (a) Micrograph of an etched 6.4 mm sample showing the spherulitic core, and sheet-like skin regions. (b) Typical micrograph of spherulite in the core of the HI-POM material. (c, d) Sheet structure of the HI-POM skin revealed in (c) fractured and (d) etched samples.

relatively large skin depth – deeper than the skin in the neat material [30] – is a consequence of the addition of the rubber, and is independent of plaque thickness. The latter finding is to be expected because the plaques were processed under similar conditions.

3.4. Tensile results

As shown in Table I, the addition of the rubber lowers the yield strength for the HI-POM material below that for the neat polymer. The finely distributed rubber particles, present in the HI-POM, serve as multiple stress concentrators and initiate crazing and shear banding at reduced stresses [1–3, 40]. Furthermore, a strong difference in strength and ductility exists between the core and skin of the HI-POM (see Fig. 6). The "core" samples fail in a relatively brittle fashion with only 25% elongation, while the "skin" is much tougher, and exhibits up to 300% elongation. In addition, the skin region strain hardens from the yield strength of 45 MPa to a failure strength of 69 MPa. In the dual layered 50/50 samples, fracture initiates in the

TABLE I Tensile data for neat and rubber-toughened polyoxymethylene tested at 12.7 mm min^{-1}

Material	Loading Direction	σ_y (MPa)	σ_{uts} (MPa)	Elongation (%)
Neat POM	Long. and Trans.	75.2	75.2	5
HI-POM				
Skin	Long	44.9	65–70	300
Skin	Trans	44.9	65–70	300
Core	Long	44.9	44.9	25
Core	Trans	42.1	42.1	25
50/50	Long	43.5	43.5	7 core 20–100 skin
50/50	Trans	38.6	38.6	7

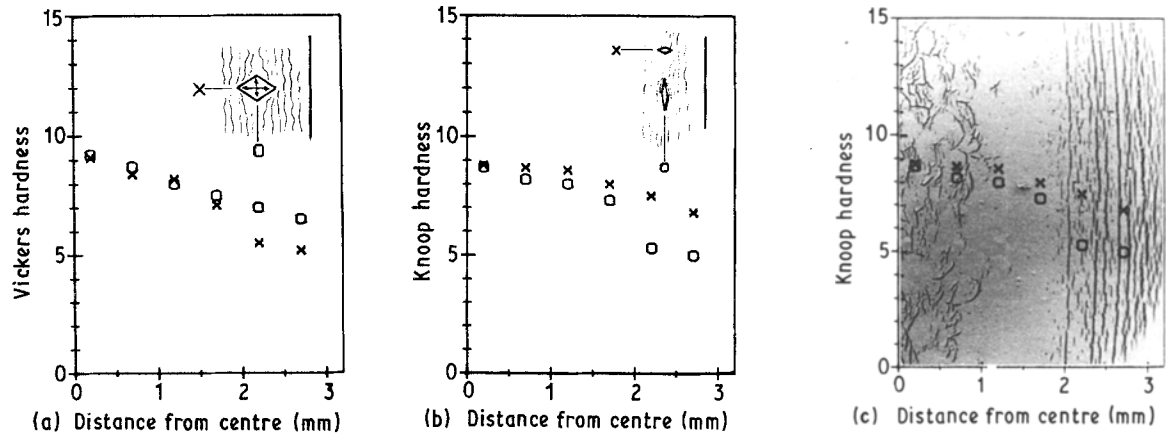

Figure 5 (a) Vickers and (b) Knoop microhardness traces across the thickness of a 6.4 mm HI-POM sample, with indentor diagonals (○) parallel and (x) normal to this direction. (c) Superposition of a Knoop microhardness trace on to the micrograph of an etched 6.4 mm HI-POM sample, correlating visual depth of skin with anisotropy in the Knoop values.

brittle core and then proceeds out towards the skin. The skin finally necks, resulting in an elongation in the range of 7% to 100%.

The differences in tensile behaviour between the core and the skin in this rubber-modified, semicrystalline system are due to one or more of the following variables: rubber content variations, rubber size and distribution, variation in the per cent crystallinity, and/or crystalline morphology. Recall that compositional characterization for the material revealed that there was no variation in either the per cent crystallinity or rubber content through the thickness; therefore the change in properties must be purely morphological in origin. In the skin, the fine rubber distribution and non-spherulitic matrix structure promote widespread shear yielding, and thus macroscopic ductility results; a drawn portion of sheet is shown in Fig. 7. Furthermore, the application of load initiates widespread delamination of the sheets, as indicated by the tentacled appearance of the fractured skin sample shown in Fig. 6. The localized biaxial stress state within these delaminated sheets also favours the predominance of a diffuse shear yielding mechanism.

By contrast, the matrix polymer in the HI-POM core may well experience a triaxial stress state within the voluminous spherulites, thereby facilitating failure through macro-crazing around the large, coarsely distributed rubber particles. Fractographs of both the 3.2 mm "core" and the 6.4 mm "50/50" samples reveal a penny-shaped region in the core within which considerable matrix drawing had occurred (Figs 8a, b). The appearances of both this drawn region and the surrounding zone are identical to the appearance of regions of stable crack growth and fast fracture, respectively, in fatigue samples. From this information, this drawn region is considered to be the initial slowly grown macro-craze, from which catastrophic fast fracture initiated.

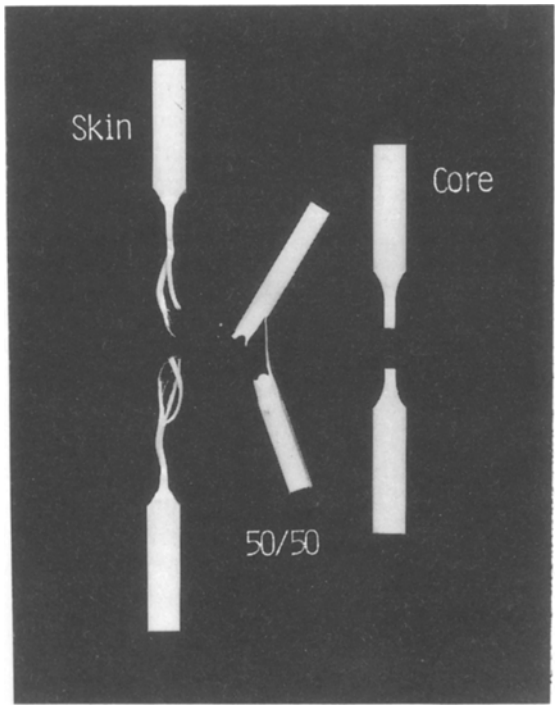

Figure 6 Typical tensile failures of the core, skin and 50/50 samples. Note the tentacled fracture appearance of the skin, the result of delamination of the individual sheets.

3.5. Fatigue behaviour

Typical fracture surfaces from fatigued samples are displayed in Fig. 9 and show a definite difference in

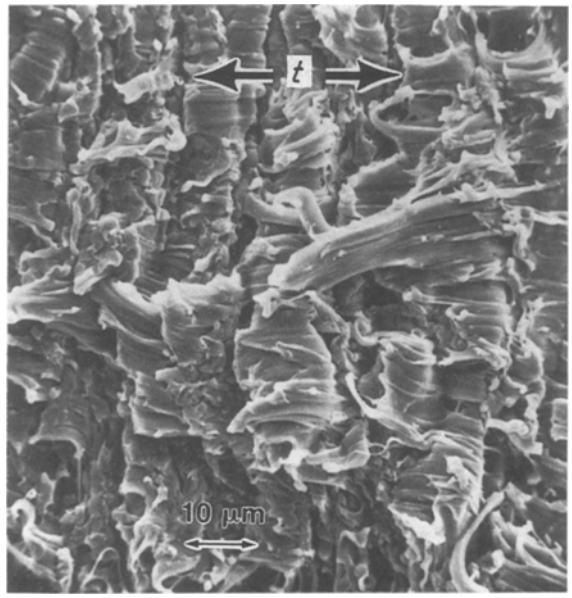

Figure 7 Ductile behaviour of the individual sheets within the skin.

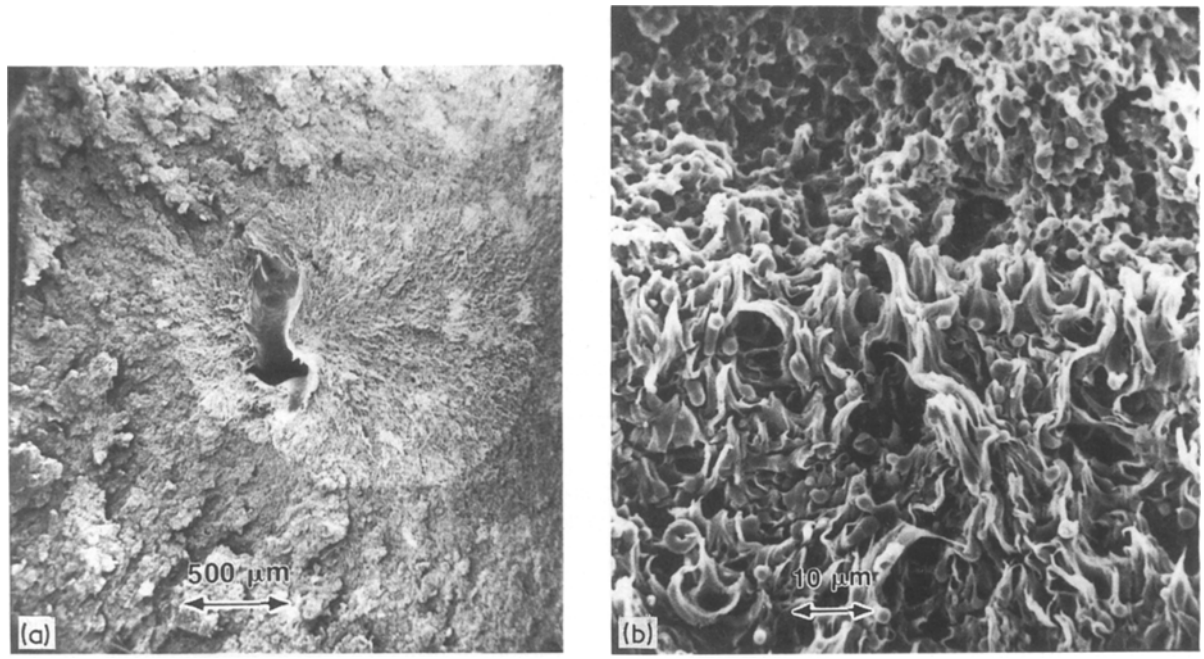

Figure 8 (a) Typical tensile fracture surface in the HI-POM core. Note the penny-shaped macrocraze which initiated brittle behaviour in the core. (b) Demarcation between (bottom) the drawn material within the macrocraze and (top) the plate-like fast-fracture region in the core of the HI-POM material.

appearance between the core and skin regions. Core fractography (Figs 9a, b) provides evidence of extensive matrix drawing in the stable crack growth regime, and a plate like-formation in the known fast fracture regime. This plate-like appearance is also found in the fast fracture regions of neat POM samples [41] and indicates a lack of matrix deformation. Also note the clear evidence for the large rubber particles present in the core region. In the skin, fatigue loading is found to delaminate the sheets, with increasing severity of delamination associated with increasing ΔK levels. Furthermore, in the skin, these sheets are found to rip out of the sample in an uneven fashion, thereby creating a contoured macroscopic fracture appearance (Fig 4c and 9c). The behaviour of the skin was found to be the same in both orientations.

Fatigue crack propagation (FCP) data are plotted in Fig. 10. While the HI-POM skin performance is improved over that of the neat resin and is isotropic, the behaviour of the HI-POM core is more complex; the curves for both the core and 50/50 samples straddle that for the neat material, with the transversely loaded sample (TL orientation) being inferior. (It is important to note that the curve for the 50/50 material is identical to that for the core, indicating that the 50/50 blend properties are dominated by the core morphology. In both fatigue and tensile samples, the normally ductile skin region only draws (under conditions that permit it to debond from the core). The anisotropy in FCP behaviour is also mirrored in the observed crack path; the cracks in the TL samples grew straight and in-plane, whereas the cracks in the longitudinally loaded (LT) samples grew straight for a short length before being diverted at 90° to the direction of the notch (Fig. 11). The bending forces present in the arms of the WOL samples are blamed for permitting the crack to grow along the weaker longitudinal plane. Therefore an SEN sample, which only applies forces normal to the notch, was used to constrain the crack in the core zone to travel in a path normal to the direction of rubber alignment. The resultant crack path, while nominally along the transverse plane, was found to be irregular and greatly tortured; much matrix drawing was observed. It is important to note that these SEN data are consistent with the limited amount of data retrieved from the LT WOL samples.

In general, it has been found that increased fatigue resistance in polymer systems is associated with increased toughness (Fig. 12a) [2, 40, 42]. The dissipation of applied cyclic energy into large plastic or damage zones reduces the potential driving force at the crack tip, and reduces the rate of crack growth. Recently, Wyzgoski and Novak [43] attempted to use a toughness criteria to identify the influences of second-phase particles on the FCP response of nylon by correlating crack growth rates with the energetic driving force for the crack, ΔG. A similar correlation has been utilized in this study. In composite/blended systems which possess varying moduli, the use of an energy-based plot provides a more rational basis for comparison of that system's FCP behaviour. Although correlating fatigue crack growth rates against ΔG does not normalize all the FCP data for a particular system, it is proposed that the use of ΔG plots permits identification of the mechanisms controlling FCP. For example, in Fig. 12b, it is shown that the TL core FCP plot is coincident with that for the neat material. This would indicate that crack gowth in this orientation is dominated by fracture within the matrix and along the matrix/particle interface. The large aligned rubber particles merely direct the crack path and do not toughen the material in this orientation; this mechanism is verified by fractographic evidence (Fig. 3a). In LT core samples, however, the rubber rods span the crack plane, and interaction with the fracture process is inevitable. In this orientation, a combination of rubber rupture, pull-out, and/or a tortured path

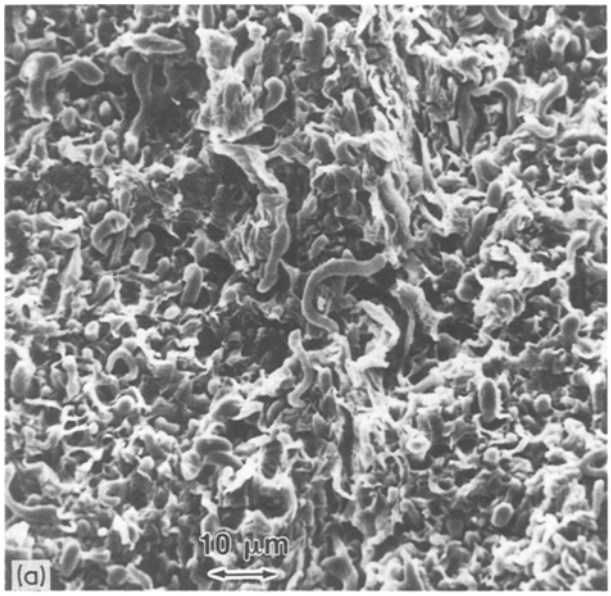

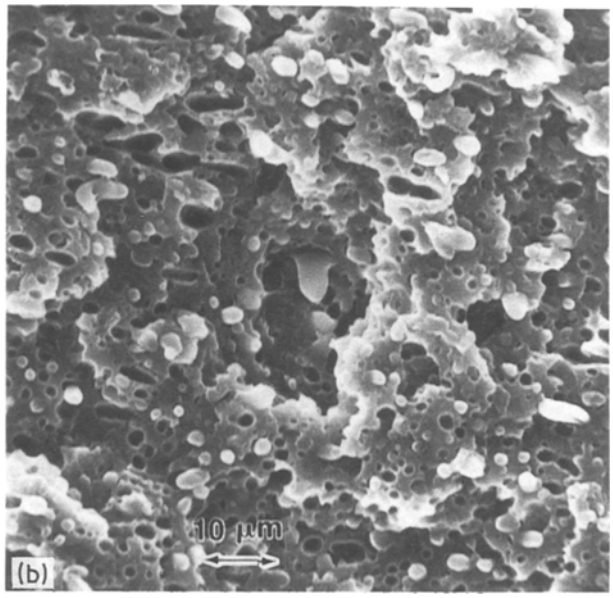

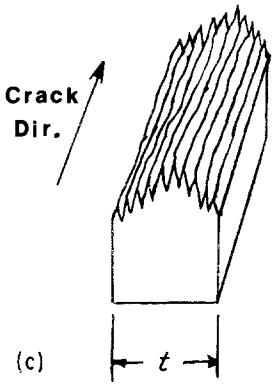

Figure 9 (a, b) Fatigue fractography in the core of the HI-POM material. (a) Stable crack-growth region ($da/dn = 2 \times 10^{-5}$ mm/cycle) demonstrating extensive matrix drawing. (b) Fast-fracture region with plate-like fracture. (c) A sketch of the contoured macroscopic fracture appearance in the skin of the HI-POM due to uneven ripping of the sheets during fatigue.

occurs, thereby improving the resistance to crack growth as shown in Fig. 12b. Note that this anisotropic FCP behaviour in the core follows the same trends as exhibited in aligned short-fibre reinforced polymer alloys [44–48]. In the HI-POM skin, two significant energy dissipative mechanisms exist: inherent ductility associated with the coordination of fine crystalline and rubber phases, and the delamination of the loosely bonded sheets. (It is the non-uniform, stick–slip nature of this delamination which creates the unusual jagged appearance of FCP response in the skin (see inset, Fig. 10)). Because neither of these energy sinks are a function of orientation, the FCP behaviour of the skin material is isotropic. Furthermore, the presence of these two toughening mechanisms improves the HI-POM skin FCP behaviour over that associated with the neat resin. This improvement in toughness is emphasized by the differences in the respective FCP curves in the ΔG–da/dn plot.

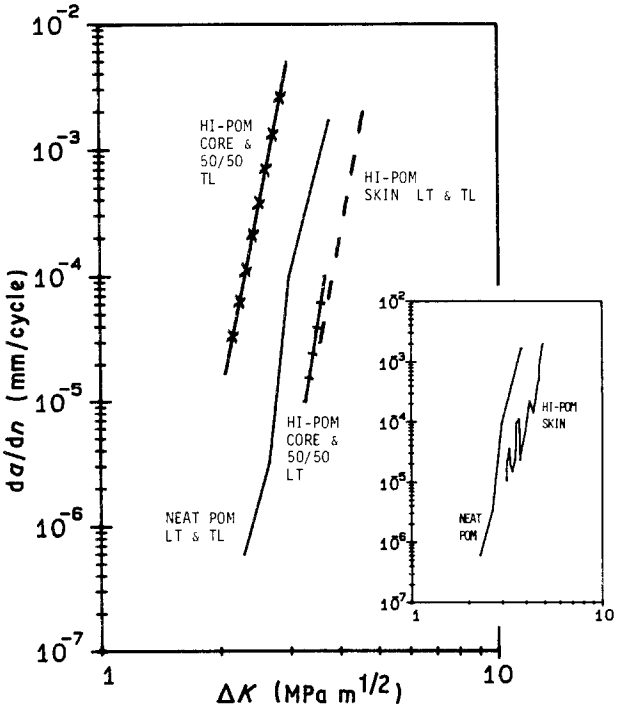

Figure 10 FCP plots for both the neat and toughened POM materials. Inset shows the jagged FCP response of the HI-POM skin material.

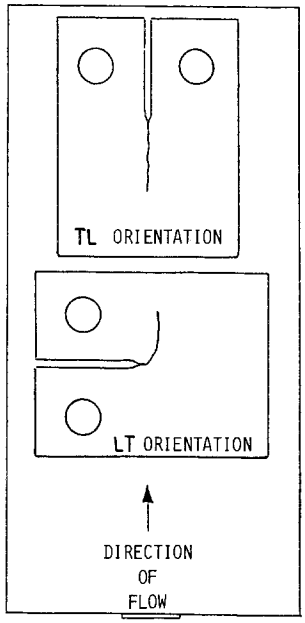

Figure 11 Anisotropy in the core of HI-POM highlighted by preferred crack paths in oriented samples.

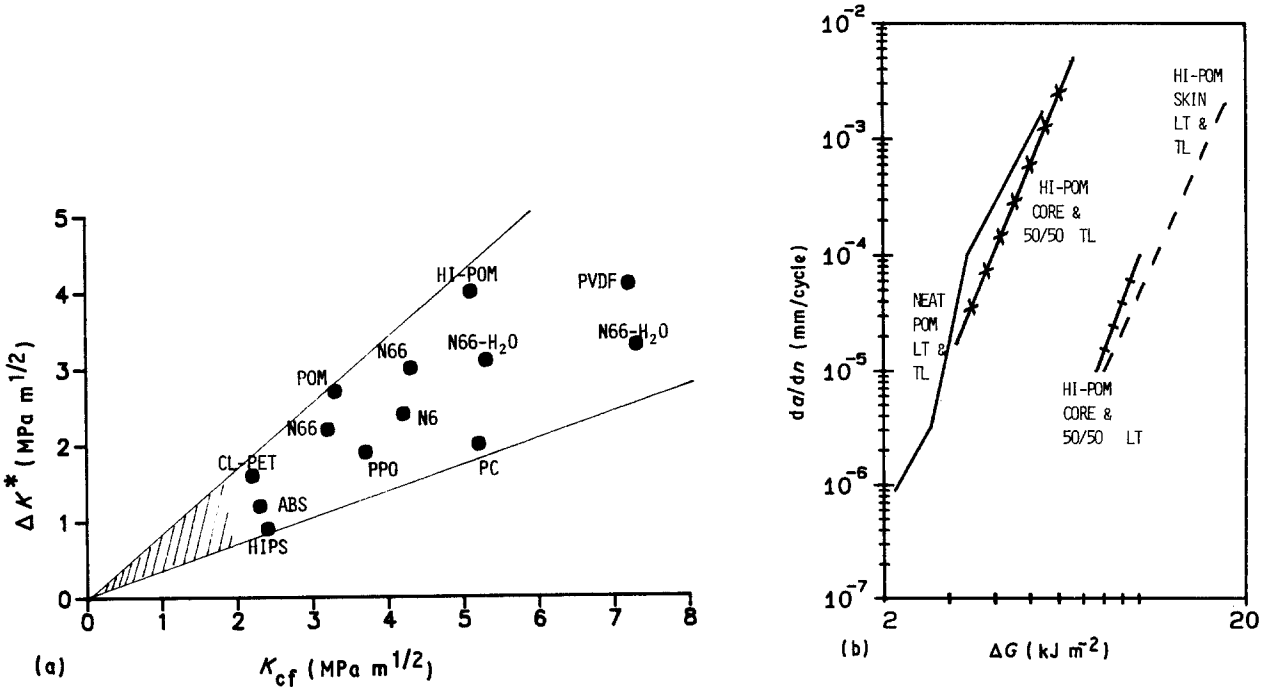

Figure 12 (a) Trends in polymer systems showing increased fatigue resistance with increased toughness. ΔK^* represents the stress intensity range required to drive a crack at a given velocity, in this case 7.5×10^{-4} mm/cycle [42]. (b) A plot of da/dn against ΔG, the range in energy release rate, for both the neat and HI-POM materials.

4. Conclusions

1. Rubber-toughened POM forms a distinct core–skin morphology when injection-moulded. The skin consists of a fine distribution of rubber and crystalline regions, arranged in 2 to 4 μm thick sheets. These sheets are stacked parallel to the mould wall, and easily delaminate under stress or when chemically attacked. By contrast, the core is composed of 100 to 300 μm POM spherulites which contain 2 to 4 μm diameter rod-like rubber particles. These large rubber particles are aligned in the direction of injection flow and are not believed to be part of an IPN structure.

2. The rubber used in ST100 is a polyurethane possessing a T_g of $-35°$ C. The matrix is 50% to 60% crystalline and the HI-POM material contains 20% to 30% rubber by weight, with the ratio of the phases being the same in both the core and skin.

3. The skin morphology exhibits ductile behaviour due to a combination of the fine rubber/matrix structure and the presence of a delamination-induced biaxial stress state. This superior ductility also accounts for improved fatigue resistance.

4. The HI-POM core morphology is embrittled by both the large rubber particles and large spherulites. In addition, the aligned rubber particles weaken the longitudinal plane, resulting in inferior tensile and fatigue properties when samples are loaded normal to the injection moulding direction.

Acknowledgements

The authors would like to express their great sadness over the passing of their colleague, Dr John Manson. His technical assistance and personal friendship will be greatly missed.

This work was funded by the E. I. DuPont de Nemours company.

References

1. A. J. KINLOCH and R. J. YOUNG, "Fracture Behaviour of Polymers" (Applied Science, New York, 1983).
2. R. W. HERTZBERG, "Deformation and Fracture of Engineered Materials", 3rd Edn. (Wiley, New York, 1989).
3. J. A. MANSON and L. H. SPERLING, "Polymer Blends and Composites" (Plenum Press, New York, 1976).
4. R. L. BALLMAN and H. L. TOOR, *Mod. Plastics* **38** (October, 1960) 113.
5. G. MENGES, G. WUBKEN and B. HORN, *Colloid Polym. Sci.* **254** (1976) 267.
6. Z. TADMOR, *J. Appl. Polym. Sci.* **18** (1974) 1753.
7. S. S. KATTI and J. M. SCHULTZ, *Polym. Engng. Sci.* **22** (1982) 1001.
8. E. S. CLARK, *SPE J.* **23** (1967) 46.
9. *Idem, Appl. Polym. Symp.* **20** (1973) 325.
10. *Idem, ibid.* **24** (1974) 45.
11. J. BOWMAN, *J. Mater. Sci.* **16** (1981) 1151.
12. R. W. LANG, J. A. MANSON and R. W. HERTZBERG, Advances in Chemistry Series no. 206 (American Chemical Society, Washington D.C., 1984) p. 261.
13. H. KESKKULA and J. NORTON, *J. Appl. Polym. Sci.* **2** (1959) 289.
14. M. FUJIYAMA and S. KIMURA, *ibid.* **23** (1979) 2807.
15. A. I. ISAYEV, *Polym. Engng. Sci.* **23** (1983) 271.
16. J. L. WHITE and J. E. SPRUIELL, *ibid.* **23** (1983) 247.
17. J. CALLEAR and J. SHORTALL, *J. Mater. Sci.* **12** (1977) 141.
18. J. BOWMAN, N. HARRIS and M. BEVIS, *ibid.* **10** (1975) 63.
19. M. J. FOLKES and D. A. RUSSELL, *Polymer* **21** (1980) 1252.
20. H. VOSS and J. KARGER-KOCSIS, *Int. J. Fatigue* **10** (1988) 3.
21. K. KATO, *Polymer* **9** (1968) 225.
22. W. J. HO and R. SALOVEY, *Polym. Engng. Sci.* **21** (1981) 839.
23. J. KARGER-KOCSIS and I. CSIKAI, *ibid.* **27** (1987) 241.
24. D. R. RUEDA, F. J. BALTA-CALLEJA and R. K. BAYER, *J. Mater. Sci.* **16** (1981) 3371.
25. K. E. PUTTICK, J. RADCLIFFE and R. D. W. WHITEHEAD, *Composites* **17** (1986) 304.

26. E. A. FLEXMAN, *Mod. Plastics* February (1985) 72.
27. *Idem,* Europ. Pat. Appl. 117664 (1984).
28. *Idem,* Europ. Pat. Appl. 120711 (1984).
29. *Idem,* Europ. Pat. Appl. 121407 (1984).
30. T. J. PECORINI, unpublished research, High University (1987).
31. D. D. HUANG, personal communication (1986).
32. Mettler TA3000 Operating Instructions (Mettler Instrumente, Switzerland, 1984).
33. ASTM D792-66, "Annual Book of ASTM Standards" (American Society for Testing and Materials, Philadelphia, Pennsylvania, 1985).
34. Metals Handbook, Vol. 11, 8th Edn. (American Society for Metals, Metals Park, Ohio, 1976).
35. ASTM D638-68, "Annual Book of ASTM Standards" (American Society for Testing and Materials, Philadelphia, Pennsylvania, 1985).
36. ASTM E399-86a, Annual Book of ASTM Standards" (American Society for Testing and Materials, Philadelphia, Pennsylvania, 1986).
37. N. G. McCRUM, B. E. READ and G. WILLIAMS, "Anelastic and Dielectric Effects in Polymeric Solids (Wiley, New York, 1967).
38. E. MARTUCHELLI, *Polym. Engng. Sci.* **24** (1984) 563.
39. M. T. HAHN, R. W. HERTZBERG and J. A. MANSON, *J. Mater. Sci.* **18** (1983) 3551.
40. R. W. HERTZBERG and J. A. MANSON, "Fatigue in Engineering Plastics" (Academic Press, New York, 1980).
41. R. W. HERTZBERG, ASTM STP 948 (American Society for Testing and Materials, Philadelphia, Pennsylvannia. 1987) p. 5.
42. P. E. BRETZ, PhD dissertation, Lehigh University (1980).
43. M. G. WYZGOSKI and G. E. NOVAK, *Polym. Preprints* **29** (1988) 132.
44. R. W. LANG, J. A. MANSON and R. W. HERTZBERG, *J. Mater. Sci.* **22** (1987) 4015.
45. M. J. CARLING, Master's Thesis, Lehigh University (1984).
46. J. F. MANDELL, F. J. McGARRY, D. D. HUANG and C. G. LI, *Polym. Compos.* **4** (1983) 32.
47. J. F. MANDELL, D. D. HUANG and F. J. McGARRY, ASTM STP 772 (American Society for Testing and Materials, Philadelphia, Pennsylvania, 1982) p. 3.
48. K. FRIEDRICH, R. WALTER, H. VOSS and J. KARGER-KOCSIS, *Composites* **17** (1986) 205.

Received 6 April
and accepted 14 September 1989